Plasma Density Measurement on an SCU-PSI Device via a CO_2 Dispersion Interferometer*)

Haoxi WANG[1,2)], Yan ZHOU[1)], Fujun GOU[3)], Yuan LI[1)], Hongbin WANG[4)], Xianjun ZHENG[4)] and Yonggao LI[1)]

[1)]*Southwestern Institute of Physics, P.O. Box 432, Chengdu 610041, China*
[2)]*Department of Engineering Physics, Tsinghua University, Beijing 10084, China*
[3)]*Sichuan University, Chengdu 610064, China*
[4)]*Hope Innovation (Shanghai) Inc., Shanghai, China*

(Received 27 November 2017 / Accepted 12 March 2018)

A new CO_2 dispersion interferometer (DI) was commissioned on the linear device at Sichuan University for the plasma surface interaction (SCU-PSI) [1]. The SCU-PSI device can generate a plasma pulse with very high density and a short duration. The DI system measured the plasma densities in several plasma discharges with rapid density changes. The results show a high correlation to other diagnostics such as the plasma current signal measured using a Rogowski coil. The line-density resolution of the system is $6.3 \times 10^{17}/m^2$. The time resolution is 0.05 ms.

Keywords: linear device, interferometer, dispersion interferometer, photoelastic modulator, pulse discharge

DOI: 10.1585/pfr.13.3402049

1. Introduction

Plasma density diagnostics are very important in the study of plasma equilibrium, stability, and confinement. The linear device at Sichuan University for plasma surface interactions (SCU-PSI) is a typical linear device, with a Langmuir probe and Rogowski coils as its diagnostic system. Due to the interaction of the probe and the plasma, the Langmuir probe is unable to measure the core density of the plasma. A dispersion interferometer (DI) system was commissioned to measure the plasma density of this device. The light source of the DI system is a 10.6-μm CO_2 laser. The system is capable of measuring the plasma density with rapid changes in the pellet injection and is insensitive to mechanical vibrations [2].

The SCU-PSI device can generate pulsed plasma with high density and short duration. A series of experiments was applied to test the DI's ability to measure such pulsed plasma.

This article discusses the density measurement by the DI system on the SCU-PSI device. A brief introduction to the SCU-PSI device is given in Section II. The principle and the modulation method of the DI system is presented in Section III, the optic layout and data acquisition of the system is given in Section IV, the experimental results are shown in Section V, and the conclusions are discussed in Section VI.

2. The SCU-PSI Device

Figure 1 shows the structure of the SCU-PSI linear device.

The device includes a plasma generation system, a vacuum system, a cooldown system, a magnetic system, and a gas puffing system. The vacuum chamber is made of stainless steel with a cooldown pipe in the chamber wall. In the experiment, argon or hydrogen gas is puffed to cascade arc plasma and a stable, low-temperature, direct current (DC) plasma is generated [3, 4]. To test the DI system's ability to measure plasma with high density and short duration, a capacitor tank applied a pulse voltage to the DC plasma, which pinches the plasma and generates a density peak. The diagnostic system on the device includes a Rogowski coil to measure the plasma current, a high-speed camera to measure the diameter of the plasma beam, and a new short-wavelength DI system to measure the plasma density.

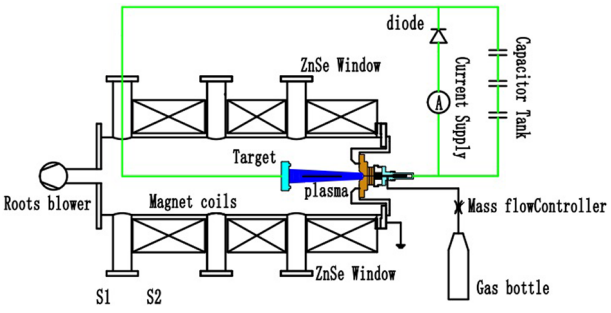

Fig. 1 The linear device at Sichuan University.

author's e-mail: wanghx@swip.ac.cn

*) This article is based on the presentation at the 26th International Toki Conference (ITC26).

3. Principle and Measurement

Figure 2 shows the basic principle of the new DIs [2, 5–10]. The CO_2 laser emits a probe beam with a frequency of ω and a vertical polarization. The beam is focused on a nonlinear crystal (SHG1), which generates a second harmonic beam with a horizontal polarization. In this experiment, a type I $AgGaSe_2$ nonlinear crystal [6] is applied. The size of the crystal is 5 mm × 5 mm × 15 mm. The conversion efficiency of the crystal is approximately 1 × 10^{-6} [2].

A photoelastic modulator (PEM) is set after the nonlinear crystal to modulate the probe beam. The core unit of the PEM is a ZnSe birefringent crystal and two piezoelectric crystals. A 50-kHz signal is translated into a pressure signal by the piezoelectric crystals. The periodic pressure on the birefringent crystal causes a sinusoidal delay only in the beam with a specified polarization direction. By adjusting the setting angle of the nonlinear crystal, only the second harmonic is modulated. The combined beam propagates through the plasma, and the phase of the beam after the plasma can be described as follows:

$$\phi_0 = \omega t + K\overline{n_e}L/\omega + 2\pi\omega\Delta l/c + \Psi_0, \quad (1)$$

$$\phi_1 = 2\omega t + K\overline{n_e}L/2\omega + 4\pi\omega\Delta l/c + g\sin(\omega_m) + \Psi_1, \quad (2)$$

where ϕ_0 and ϕ_1 are the phases of the fundamental beam and the second harmonic, respectively, $K = e^2/(2\epsilon_0 m_e c)$, which is a constant, the terms $K\overline{n_e}L/\omega$ and $K\overline{n_e}L/2\omega$ are the phase shifts caused by the plasma, and the terms $2\pi\omega\Delta l/c$ and $4\pi\omega\Delta l/c$ are the phase shifts caused by an optical length change of Δl due to mechanical vibrations. The phase shift caused by PEM is $g\sin(\omega_m t)$, where g is the adjustable maximum phase shift of the modulator and ω_m is the modulation frequency. Ψ_0 and Ψ_1 are the initial phase differences of the fundamental beam and the second harmonic, respectively.

The beam is focused on the second nonlinear crystal (SHG2) after the plasma to generate another second harmonic. The phase can be described as follows:

$$\phi_2 = 2\omega t + 2K\overline{n_e}L/\omega + 4\pi\omega\Delta l/c + 2\Psi_0. \quad (3)$$

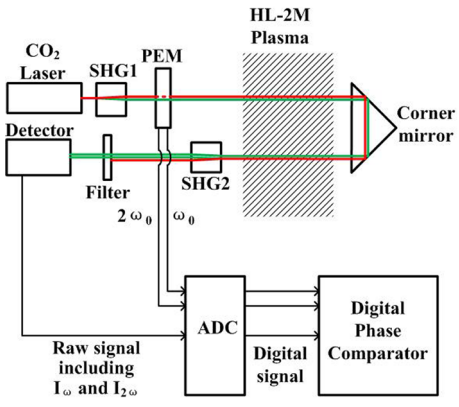

Fig. 2 Conceptual design of the dispersion interferometer.

The fundamental wave is eliminated by a filter after the second nonlinear crystal. The two second harmonics are combined and detected by the infrared detector, which is only sensitive to the second harmonic. The beam received by the detector can be described as follows:

$$I = A + B\cos[\phi_2 - \phi_1] = A + B\cos[3K\overline{n_e}L/2\omega - g\sin(\omega_m t) + \Psi]. \quad (4)$$

The component caused by mechanical vibration is eliminated.

The signal can be Fourier expanded as follows:

$$\begin{aligned} I &= A + B\cos(3K\overline{n_e}L/2\omega + \Psi)\cos[g\sin(\omega_m t)] \\ &\quad + B\sin 3K\overline{n_e}L/2\omega + \Psi)\sin[g\sin(\omega_m t)] \\ &= A + B\cos(3K\overline{n_e}L/2\omega + \Psi) \\ &\quad \times\left[J_0(g) + 2\sum_{n=1}^{\infty} J_{2n}(g)\cos(2n\omega_m t)\right] \\ &\quad + 2B\sin(3K\times\overline{n_e}L/2\omega + \Psi) \\ &\quad \times\sum_{n=1}^{\infty} J_{2n-1}(g)\sin[(2n-1)\omega_m t], \end{aligned} \quad (5)$$

where J_n refers to a Bessel function of the first kind.

The amplitudes of the fundamental and the second harmonic components of ω_m are

$$I_{\omega_m} = 2B\sin(3K\overline{n_e}/2\omega + \Psi)J_1(g), \quad (6)$$

$$I_{2\omega_m} = 2B\cos(3K\overline{n_e}L/2\omega + \Psi)J_2(g). \quad (7)$$

We set g to 2.6 to make $J_1(g) = J_2(g)$ so that the average density is

$$\overline{n_e} = \left(\arctan^{-1}\frac{I_{\omega_m}}{I_{2\omega_m}} - \Psi\right)\times 2\omega/3KL. \quad (8)$$

I_{ω_m} and $I_{2\omega_m}$ can be extracted by software from the raw signals, and $\overline{n_e}$ can be obtained.

4. Optical Layout and Data Acquisition

Figure 3 shows the optical layout on the linear device. Two ZnSe windows are located on opposite sides of the chamber. The probe beam crosses the plasma beam vertically. The aperture of the windows is 50 mm. The distance between the two windows is 760 mm.

There is only one 1 m × 2 m optic table set at one side of the device. A reflector is needed to reflect the probe beam back to the optic table. If a corner cube retroreflector is applied, the incident beam and the returning beam will be parallel. Due to the small aperture of the windows, the two beams will be too close to separate. Therefore, a concave mirror is applied as a reflector and there is a small angle (1.5°) between the two beams separating them. Most of the optical components of the interferometer system are set on the optic table. The concave mirror F2 is set on an individual frame at the opposite side of the device.

The elevation of the optic table is much lower than the windows on the vacuum chamber; therefore, a beam

steerer is applied to adjust the elevation of the laser beam. The beam is focused by the mirror F1 with a beam waist at the center of SHG1. The beam passes through the vacuum chamber and is reflected and focused on SHG2 by the mirror F2. The mirror F3 focuses the beam on the detector.

A paraxial approximation is applied in the optic design so that the beam and the beam transformation are assumed to be Gaussian. A concave mirror with a 1-m focal length is applied to transform the beam parameters to match the aperture of the incident window. The total optical length of the system is 8.354 m.

Figure 4 shows how the beam radius varies in the system. The vertical lines F1–F3 mark the positions of the three concave mirrors. The vertical lines SHG1 and SHG2 mark the positions of the two nonlinear crystals. The waist radius of the output laser beam is 1.25 mm. The beam radius at the center of the vacuum chamber is 7.27 mm. The beam radius at the ZnSe window is 5.366 mm at the first window and 9.147 mm at the second window. The distance between the incident beam and the outgoing beam at the incident window is 21 mm. Considering the power loss on the mirror, the aperture should be larger than 2.2 times the beam diameter. The necessary aperture is $5.366 \times 2 \times 2.2 + 21 \approx 44.6$ mm, which is smaller than the actual aperture of the ZnSe window (50 mm).

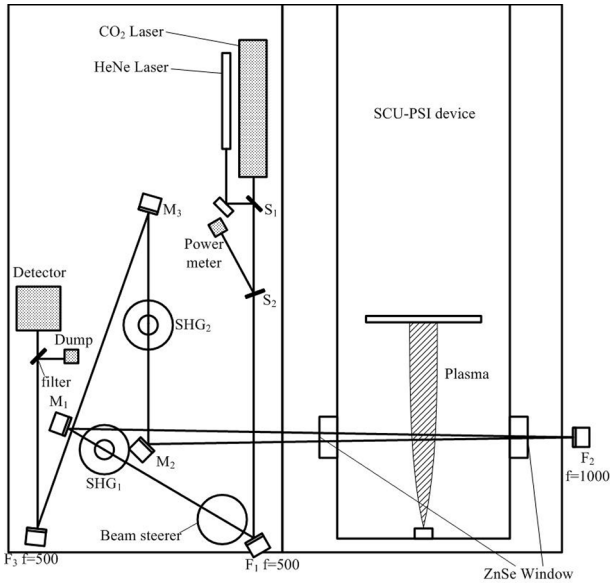

Fig. 3 Optical layout of the dispersion interferometer on the linear device.

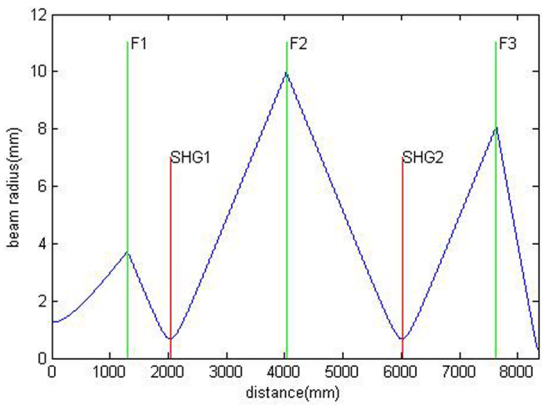

Fig. 4 Beam radius in the DI system on the linear device.

A digital phase comparator is applied for data processing. I_{ω_m} and $I_{2\omega_m}$ can be calculated from the raw signal and the reference signal produced by the PEM.

5. Experimental Results

In the SCU-PSI device, a high-density pulsed plasma can be observed when a pulse voltage is applied to the DC plasma. The plasma density in the pinch is measured in the experiments.

Figure 5 shows how the plasma density changes in the experiment. Because it takes too long to establish the DC plasma (up to 10 s), it is difficult for the DI system to cover the entire procedure. To measure the density peak, the density of the DC plasma and the density change in the pinch are measured separately.

To calculate the average density, the average optical length in the plasma is calculated via numerical integration. The average optical length can be fitted linearly as

$$L = 2.15 \times D - 6\,\text{mm}. \tag{9}$$

5.1 Density of the DC plasma

The density of the DC plasma is determined by the gas type and the gas flow in the discharge. In this experiment, the gas type is set to argon and the gas flow is set to 300 SCCM. To measure the density of the DC plasma, the plasma is established and the magnetic field is shut down at a certain time. The entire shutting down procedure is measured by the DI system. The falling edge indicates the background density.

Figure 6 shows the phase shift caused by the falling edge. The phase shift is approximately 6.6°. The diameter of the cross section of the DC plasma beam is approximately 15 mm. The average optical length of the probe beam in the DC plasma is 26.25 mm according to Equation (9). According to Equation (8), the average plasma density in the DC plasma beam is $0.983 \times 10^{20}/\text{m}^3$.

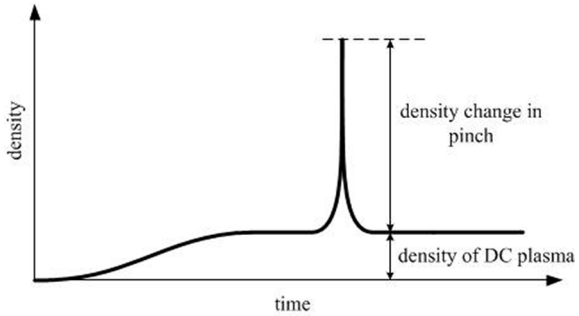

Fig. 5 Plasma density in the experiment.

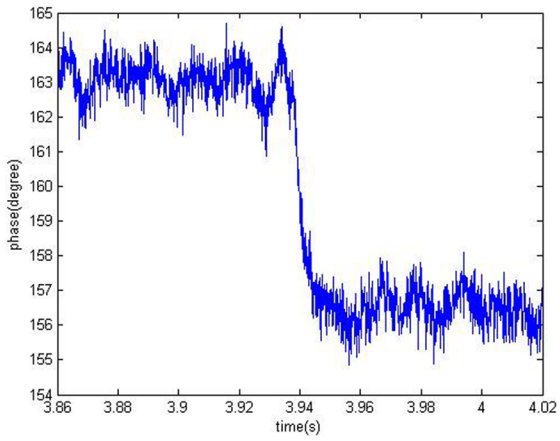

Fig. 6 Falling edge of the background density measured by the DI system (gas type: argon; gas flow: 300 SCCM).

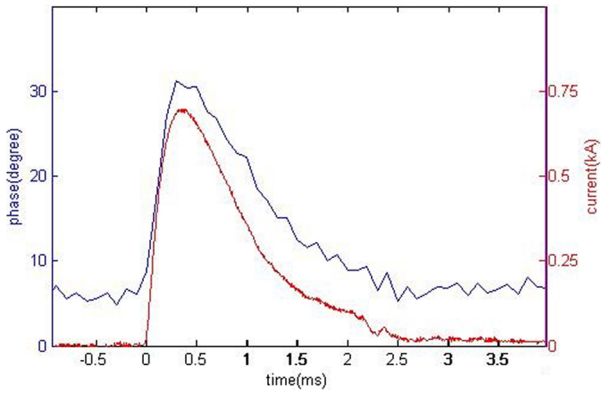

Fig. 7 Phase and current variations during a pulse (shot 10309). The phase of the DC plasma density (6.6°) is added to the curve (gas type: argon; gas flow: 300 SCCM).

5.2 Plasma density in the pinch

Figure 7 shows the phase signal of the DIs and the current variations during a plasma pinch. A 0.7-kA peak current occurs during the pinch. The variation of the phase signal shows a high correlation with the current signal. The phase resolution in Fig. 7 is 1.6°, which corresponds to a line-density resolution of $6.3 \times 10^{17}/\mathrm{m}^2$. This resolution is sufficient for the linear device, whose plasma line-density is up to $40 - 200 \times 10^{17}/\mathrm{m}^2$.

Figure 8 shows the density calculated from the line-density data and the diameter data according to Equation (9). The diameter of the plasma beam was measured using a 100-kHz high-speed camera. When the plasma current is not sufficiently high, the brightness of the plasma beam decreases and the camera cannot distinguish the edge of the beam. Therefore, diameter data can only be acquired when the plasma current is high.

The time resolution of the DI system depends on the digital phase comparator and is limited by the modulation frequency. The time resolution in Figs. 7 and 8 is 0.05 ms, while a typical peak width of a pinch in the linear device is 2 - 3 ms.

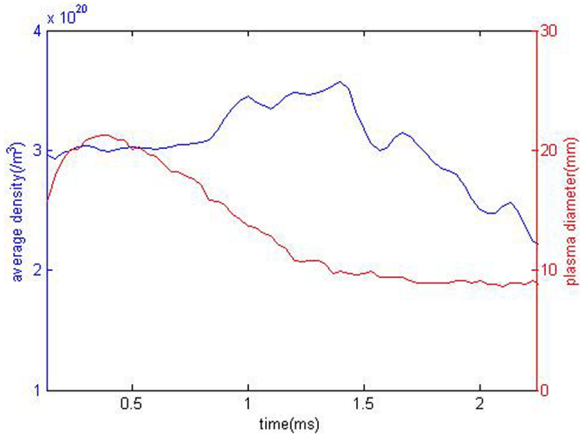

Fig. 8 Diameter and density of the plasma during a pulse (shot 10309). (gas type: argon; gas flow: 300 SCCM).

6. Summary

The experimental result shows the capability of the DI system to measure a density peak of short duration. The time resolution of the DIs is sufficient for a density peak whose duration is only 2 - 3 ms.

Acknowledgements

The authors are grateful to Wei Jin for his support in device experiment, to Dr. Zhihui Huang for his video recording using a high-speed camera, to Xiaoquan Ji and his team for current measurement. This work is supported by the National Magnetic Confinement Fusion Science Program (No. 2014GB109001), National Natural Science Foundation of China (Grant Nos. 11275059 and 11505053).

[1] X.C. Ma, X.G. Cao, L. Han, W.X. Xia, L. Shu, P.N. He and F.J. Gou, Nucl. Fusion Plasma Phys. **37**, 267 (2017).
[2] X. Wang, Y. Zhou, Y. Li, Y.H. Li and J. Yi, Rev. Sci. Instrum. **88**, 103502 (2017).
[3] X. Cao, W. Ou, S. Tian *et al.*, Fusion Eng. Des. **89**, 2864 (2014).
[4] X. Cao, S. Chen, W. Zhang *et al.*, Fusion Eng. Des. **89**, 2929 (2014).
[5] T. Akiyama, K. Kawahata, S. Okajima and K. Nakayama, Rev. Sci. Instrum. **81**, 10D501 (2010).
[6] D.L. Brower, Y. Jiang, W.X. Ding, S.D. Terry, N.E. Lanier, J.K. Anderson, C.B. Forest and D. Holly, Rev. Sci. Instrum. **72**, 1077 (2001).
[7] T. Akiyama, K. Kawahata, S. Okajima and K. Nakayama, Plasma Fusion Res. **5**, S1041 (2010).
[8] P.A. Bagryanskii, V.P. Drachev and Yu. I. Krasnikov, Sov. J. Plasma Phys. **18(2)**, 138 (1992).
[9] P.A. Bagryansky *et al.*, Rev. Sci. Instrum. **77**, 053501 (2006).
[10] J. Flieser, A. Morozov, T. Neger and H. Jager, Appl. Phys. **29**, 2413 (1996).